Journal of Materials Chemistry A

The nickel battery positive electrode revisited: stability and structure of the β-NiOOH phase

Journal:	*Journal of Materials Chemistry A*
Manuscript ID	TA-ART-08-2018-007460.R1
Article Type:	Paper
Date Submitted by the Author:	20-Sep-2018
Complete List of Authors:	Casas-Cabanas, Montse; CIC energiGUNE, Radin, Maxwell ; University of California Santa Barbara, Materials Department Kim, Jongsik; Northwestern University, Chemical Engineering Grey, Clare; University of Cambridge, Chemistry Department Van der Ven, Anton; University of California Santa Barbara, Materials Department Palacín, M. Rosa; Institut de Ciencia de Materials de Barcelona

Journal Name

ARTICLE

The nickel battery positive electrode revisited: stability and structure of the β-NiOOH phase.

Received 00th January 20xx,
Accepted 00th January 20xx

DOI: 10.1039/x0xx00000x

www.rsc.org/

Montse Casas-Cabanas,[a]* Maxwell D. Radin,[b] Jongsik Kim,[c, †] Clare P. Grey,[c,d] Anton Van der Ven,[e] M.Rosa Palacín[f,]*

The crystal structure of the nickel battery positive electrode material, β-NiOOH, is analyzed through a joint approach involving NMR and FTIR spectroscopies, powder neutron diffraction and DFT calculations. The obtained results confirm that structural changes occur during the β-$Ni(OH)_2$/β-NiOOH transformation leading to a metastable crystal structure with a TP2 host lattice. This structure involves two types of hydrogen atoms both forming primary and secondary hydrogen bonds. The formation of TP2 NiOOH as opposed to the more stable P3 host type during β-$Ni(OH)_2$/β-NiOOH transformation has a kinetic origin that can be understood by a lower strain penalty involved in the transformation.

Introduction

Nickel batteries were conceived around the turn of the 19th century using nickel hydroxide as the positive electrode and either cadmium or iron as the negative electrode.[1–4] Since the chemistry of these cells can be complex, especially for the positive electrode, incremental improvements in performance were empirically driven. This paved the way for the continuous development of cells that were able to embrace emerging applications such as spacecraft (Ni/H_2 cells developed between the 1970s and 1980s), portable electronics and ultimately hybrid electric vehicles (Ni/MH). Indeed, they fulfil the basic requirements needed in industrial and transportation applications in terms of energy density, charge-discharge rate, lifetime, cost, and safety. In parallel with such technological developments, emphasis was also placed on achieving chemical understanding of the processes taking place during charge and discharge.[5] The positive electrode contains layered brucite-type β-$Ni(OH)_2$ in the discharged (reduced) state and β-NiOOH in the charged (oxidized) state. Electrode manufacturers empirically established more than fifty years ago that as-precipitated nanometric β-$Ni(OH)_2$ exhibited higher capacity than well crystallized β-$Ni(OH)_2$, representing one of the first realizations of the beneficial effects of using nanomaterials for battery performance.[6] Nonetheless, it was not until the end of the past century that the origin of this improved electrochemical activity was analyzed from a fundamental point of view.[7,8] As a consequence, it is now generally accepted that a shorter ion/electron diffusion length coupled with strains and structural defects are sine qua non reasons for electroactivity.[9–12] Another elusive question deals with the crystal chemistry of the phases involved and the phase transformations induced by the redox processes taking place during battery functioning. Four different phases can be involved in the nickel oxyxydroxide electrode, as described by Bode in 1969:[13] α-$Ni(OH)_2$ and β-$Ni(OH)_2$ in the reduced state and β-NiOOH and γ-NiOOH in the oxidised state. The structures of all these phases consist of a stack of layers of edge sharing NiO octahedra parallel to the c-axis, differing only in their stacking sequence, the distance between the layers and the amount of intercalated species, if any. Among them, only β-$Ni(OH)_2$ is a well characterized, highly crystalline compound, isostructural with brucite (space group P-3m1), with a T1 structure (ABAB oxygen stacking sequence and hydrogen in a tetrahedral environment).[7] When oxidised upon battery charge, a transformation takes place to yield poorly crystallised β-NiOOH, exhibiting only one intense diffraction peak.[10] In the absence of reliable structural information for this phase, the high reversibility of the redox transfer and the very good cycle life exhibited by nickel based batteries led to the general assumption that β-NiOOH was isostructural with β-$Ni(OH)_2$.[13,14] Upon further oxidation of the positive electrode, a transformation of β-NiOOH to the "so-called" γ-NiOOH phase takes place. γ-NiOOH refers to a relatively poorly characterised family of compounds with differing amounts/types of intercalated alkaline ions and water but exhibiting higher crystallinity. The structural determination of a single crystal of composition $Na_{0.33}Ni(H_2O)_{0.67}O_2$ revealed a P3 structure (ABBCCA stacking with hydrogen atoms in

[a] CIC energiGUNE, Albert Einstein 48,01510 Miñano, Álava, SPAIN
[b] Materials Department, University of California, Santa Barbara, CA 93106, USA
[c] Chemistry Department, Stony Brook University, NY 11794-3400, USA
[d] Chemistry Department, Cambridge University, Lensfied Rd., CB2 1EW, UK
[e] Institut de Ciència de Materials de Barcelona (CSIC), Campus UAB E-08193 Bellaterra, Catalonia, SPAIN
† present address Department of Chemistry, Dong-A University, Busan, 604-714, KOREA
Electronic Supplementary Information (ESI) available: ^2H NMR spectra and XRD patterns of aged β-NiOOH and a discussion of NMR spectra assignments.

prismatic sites).[15] Reduction of γ-NiOOH leads to metastable α-$Ni(OH)_2$, that also accommodates anions and exhibits a turbostratic structure.[16] The common belief that the β-NiOOH phase is isostructural with β-$Ni(OH)_2$ (T1 with ABAB oxygen layer stacking sequence) has been recently dismissed. Investigations on the phase stability of nickel oxyhydroxides from first principles calculations using density functional theory (DFT) predicted that a P3 host structure (with AABBCC stacking) was favoured thermodynamically with respect to T1.[17] This result, although surprising in view of the good reversibility of the redox couple, would be in agreement with β-NiOOH being isostructural with γ-NiOOH and β-CoOOH. In parallel with these studies, the structural characterisation of β-NiOOH was carried out through a combined HRTEM-powder diffraction approach.[18] Despite the very low crystallinity of this phase, HRTEM observations showed evidence of long-range order covering a few unit cells with doubling of the c-axis, which is consistent with a weak reflection in the XRD pattern at d 9.3 Å already reported in old publications.[13] Simultaneous consideration of structural and microstructural models made a Rietveld refinement of the average crystal structure using neutron and X-ray diffraction data possible. The results confirmed that the host structure of β-NiOOH exhibited ABCA stacking instead of the expected T1 (ABAB); validating the hypothesis formulated from DFT calculations that significant structural changes were taking place in the electrode under battery operation. However, experimental evidence of the exact number and location of hydrogen environments has not been reported to date, and therefore the crystal structure of β-$Ni(OH)_2$ has astonishingly not been fully determined yet. The ABCA stacking sequence exhibits two types of interlayers: one with prismatic sites (between AA oxygen sheets), and the other exhibiting both tetrahedral and octahedral sites (between BC sheets). This implies that if hydrogen atoms are present in both types of interlayers (which would lead to either a TP2 or a OP2 host type) their positions are not necessarily equivalent as is the case for the parent β-$Ni(OH)_2$, which might have important implications in view of the renewed interest of β-NiOOH as one of the most promising catalysts for water splitting.[19–21] In order to discriminate between both structural types, precisely locate hydrogen atoms in the structure and understand the underlying factors leading to the formation of this polytype instead of the P3 phase predicted to be more stable, we joined efforts and combined IR, NMR and neutron diffraction studies with first principles calculations. The obtained results provide a framework for understanding apparent discrepancies found in recent literature,[22–26] shed light into the mechanisms governing the redox transformations occurring at the positive electrode during nickel battery operation and are expected to positively contribute to the rationalization of the successful catalytic activity of β-NiOOH.

Experimental and computational methods

Synthesis

Since γ-NiOOH impurities are easily formed during oxidation of β-Ni(OH)2 when alkaline ions are present in the reaction medium, a dry synthetic route using ozone as oxidizing agent[27] was chosen to prepare pure β-NiOOH for structural investigations. Ozone was generated in a BMT 803 system from a pure oxygen source (99.995%) flow (0.8 l/h) and forced to pass through a vertical reactor containing typically 1 g of the industrial commercial β-Ni(OH)2 (Friwo GmbH) precursor on a sinter. Residual ozone not consumed in the reaction was conducted to a reducing solution containing sodium thiosulfate and potassium iodide acting as an indicator. The progress of the reaction was followed by taking a very a small amount of sample every hour that was analyzed by infra-red spectroscopy (FTIR). Preparation of fully deuterated samples was attempted by ion exchange, through treatment of β–NiOOH in D2O for 12h. D/H exchange occurred as a result of moisture in the air (despite keeping the samples in desiccators) and so all the samples were re-ion exchanged in D2O prior to the NMR experiments. The samples were then dried under vacuum for 12 hours and packed in NMR rotors in a glove box.

Chemical analysis

The total nickel content was determined by complexometric ethylenediaminetetraacetic acid (EDTA) titration and its oxidation state by iodometry. The analyses were repeated twice. Typically ca. 80 mg of sample are mixed with 3 g KI and dissolved in 100 ml of acetic acid/sodium acetate buffer solution. The I_2 produced due to nickel reduction is titrated with 0.05 M $Na_2S_2O_3$ using starch as indicator. 200 ml distilled water and 28 ml NH_3 (30%) are then added to the solution and complexometric titration is carried out with 0.05 M EDTA using murexide as indicator.

FTIR Spectroscopy

IR spectra were recorded using a Perkin Elmer Spectrum One FTIR spectrophotometer and were performed on pellets made by mixing a small amount of sample with KBr that had been previously dried at 125 ◦C.

MAS (Magic Angle Spinning) NMR

^{2}H MAS NMR experiments were performed on a CMX-200 spectrometer using a 1.8 mm Samoson probe with a 34 kHz spinning frequency. A rotor-synchronized, spin-echo pulse sequence was used with a pulse delay of 0.2 s and the ^{2}H NMR spectra were referenced to D_2O at 4.8 ppm. The relative intensities of the different environments were determined by deconvolution of the isotropic resonances and their corresponding spinning sidebands.

Structural Rietveld refinement

Neutron powder diffraction (NPD) data were obtained using the 3T2 high-resolution diffractometer at the Laboratoire Léon Brillouin (LLB), at λ = 1.224 Å with a step size of 0.05º on a 2θ

domain ranging from 1º to 125º. The instrumental resolution function (IRF) was determined with a $Na_2Ca_3Al_2F_{14}$ standard (U = 0.204186 deg^2, V = -0.300065 deg^2, W = 0.157004 deg^2). Rietveld refinements were carried out with the program FullProf[28] (Windows version, May 2009) using the pseudo-Voigt profile function of Thompson, Cox and Hastings.[29] In a previous paper[18] we reported the results obtained in a combined NPD and XRD refinement in order to refine the profile parameters concerning anisotropic strains and size accurately, with a preset weighting factor of 0.6:0.4 respectively. In order to get further insight in the position of hydrogen atoms a new series of Rietveld refinements were performed only with NPD data. Because of the poor crystallinity of the sample, profile parameters were fixed to the values obtained in the combined NPD+XRD refinement in order to minimize the number of refined parameters.

First-principles computation

Density Functional Theory (DFT) was used to calculate the energies of a variety of structures in the NiOOH-$Ni(OH)_2$ system. DFT calculations were performed with the VASP plane-wave code[30–33] using the optb86b-vdW exchange-correlation functional.[34–36] To capture the effects of electron correlation on d orbitals, the calculations employed the on-site Coulomb correction of Dudarev *et al*. with U_{eff} = 5.5 eV for Ni.[37] Similar values for U_{eff} have been used previously in related compounds.[22,23,38] The core states of the Ni, O and H ions were treated with the projector augmented wave method.[39] All calculations were performed with an energy cutoff of 600 eV. As k-point sampling, we used an grids with a minimum density of 38 Å. For T1-$Ni(OH)_2$, this corresponded to a 9 × 9 × 5 grid. Relaxations were performed using a Gaussian smearing of width 0.1 eV, while final energies were calculated using the tetrahedron method with Blöchl corrections.[40]

Symmetrically distinct orderings were enumerated using the Clusters Approach to Statistical Mechanics (CASM) software package.[41–44] For the P3 structure, configurations were enumerated over all hydrogen off-centering degrees of freedom, with the composition restricted to x = 0 in $NiOOH_{1+x}$. For TP2, we enumerated over all off-centering degrees of freedom in the P3 layer and hydrogen/vacancy degrees of freedom in the T1 layer. To account for the Jahn-Teller distortion of the Ni^{3+} ions, both the P3 and TP2 enumerations were performed in a cell in which the threefold symmetry was broken. Because many of the TP2 configurations at x = 0 relaxed to P3 structures, we employed the structure mapping algorithm implemented in CASM[41–44] to determine whether each relaxed TP2 configuration belonged to the P3 or TP2 host.

Overview of crystallography

The hydrogen atoms of T1 β-$Ni(OH)_2$ (ABAB stacking sequence), occupy sites within the intercalation layers that are tetrahedrally coordinated by oxygen. The hydrogen ions, however, are not exactly centered within the tetrahedral sites, but are tightly bound to one oxygen, forming a primary H-O bond that points towards the center of the tetrahedral site, as illustrated in Figure 1 (a).

A first-principles investigation of phase stability in the $Ni(OH)_2$-NiOOH system predicted a change in stacking sequence of the NiO_2 slabs as hydrogen is removed from T1 $Ni(OH)_2$.[17] The thermodynamically favored crystal structure for NiOOH has a P3 stacking sequence of the NiO_2 slabs, which is equivalent to an AABBCC stacking sequence of the close-packed oxygen planes. The intercalation layers accommodating hydrogen are between the AA, BB and the CC oxygen layers, which form prismatically coordinated sites. The hydrogen atoms in P3 NiOOH are predicted to occupy off-centered sites on the edges of prisms as illustrated in Figure 1 (b). The off-centering arises from an energetic preference of hydrogen to form a short primary H-O bond with the oxygen above (below) it and a longer secondary H-O bond with the oxygen below (above) it. There are many ways to distribute the primary and secondary bonds within the intercalation layers of P3.

As mentioned above, the crystal structure β-NiOOH was found experimentally to consist of an ABCA stacking sequence of close packed oxygen planes and can thus be considered to be an intermediate between T1 and P3 structures (see the three polytypes in Figure 2). The interlayer between the AA planes has the same local environment as the P3 structure, allowing the formation of linear primary and secondary H-O bonds, while the interlayer between the BC planes has the same local environment as the T1 crystal structure, in which hydrogen can reside in either tetrahedral or octahedral sites. While the P3 polytype could only accommodate one hydrogen per Ni ion, both the TP2 and OP2 structure, having an ABCA oxygen-stacking sequence, would be able to incorporate up to 1.5 hydrogen atoms per Ni, as the layer between the BC planes has two tetrahedral and two octahedral sites for every Ni. Thus, full occupancy of the tetrahedral / octahedral and prismatic edge sites in the TP2 or OP2 polytypes is consistent with $NiOOH_{1.5}$ stoichiometry, which indicates that the structure of β-NiOOH should contain hydrogen vacancies.

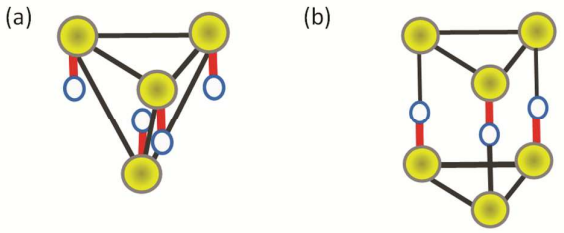

Figure 1. Local environments for hydrogen atoms in the intercalation layers of the T1, P3 and TP2 crystal structures (white and yellow atoms represent H and O). Hydrogen atoms prefer to form short primary H-O bonds (in red). (a) In the T environment (between AB stacking of close-packed oxygen planes), the hydrogen atoms reside close to the center of oxygen tetrahedra; (b) in the P environment (between AA stacking of close-packed oxygen planes), the hydrogen atoms occupy sites on the edges of oxygen prisms.

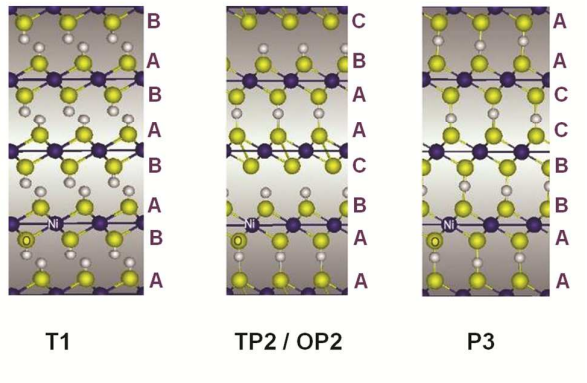

Figure 2. Crystal structures of T1-Ni(OH)2, P3-NiOOH and OP2/TP2-NiOOH. Stacking sequences of the close packed oxygen planes are also labeled. White, yellow and purple atoms represent H, O and Ni.

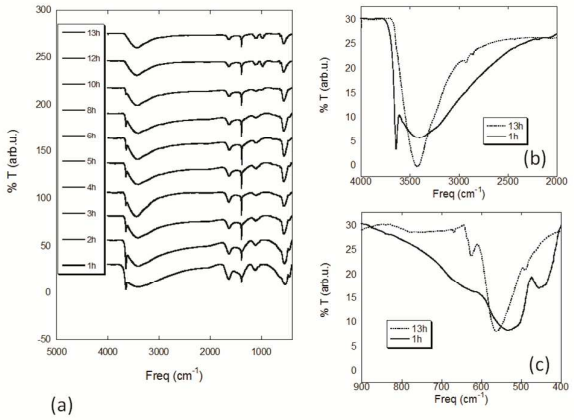

Figure 3 a) FTIR spectra recorded at 1h intervals in the course of ozonation of β-$Ni(OH)_2$. Expanded high frequency (b) and low frequency (c) regions for pristine β-$Ni(OH)_2$ and final β-NiOOH.

Results and discussion

FTIR

FTIR was found to be especially well suited to follow the β-$Ni(OH)_2$ oxidation reaction to yield β-NiOOH and allow a very fast discrimination between both phases, being much more sensitive than XRD.[45] Spectra from samples in the course of oxidation (see Figure 3(a)) show progressive intensity decrease for the sharp band at 3650 cm^{-1}. This band corresponds to the stretching of the non-hydrogen bonded hydroxyl groups[46] and is found to completely disappear after 12h in agreement with the achievement of full oxidation to β-NiOOH (see Figure 3 (b) for an expanded high frequency region for the pristine β-$Ni(OH)_2$ and the fully oxidised β-NiOOH). Therefore, FTIR results point conclusively towards full hydrogen bond formation. Linear hydrogen bonds can be formed if hydrogen atoms in the AA interlayer of an ABCA stacking sequence are off-centered, as predicted from DFT.[17] However, none of the possible coordination geometries for the BC interlayer would allow linear hydrogen bonding to exist. Nonetheless off-centering and deviation of ideal positions (as predicted from DFT for the P3 structure), cannot be ruled out.

Figure 3(c) shows the expanded low frequency region for the pristine β-$Ni(OH)_2$ and the fully oxidised β-NiOOH in which additional differences can be observed. The Ni-O lattice mode at 456 cm^{-1} is no longer observed in the oxidised phase, and the formation of hydrogen bonds is again detected by the shift of the *in-plane bending* band of hydroxyl groups from 530 cm^{-1} to 560 cm^{-1}.[46]

Chemical analysis

The oxidation degree of nickel in fully oxidised β-NiOOH was analysed through iodometric/complexometric titration yielding 2.93, slightly lower than the expected 3 value. Considering that the uncertainty estimated from direct repetitions of the measurement was found to be very low (0.01%) and that values lower than three have been previously reported for pure β-NiOOH with diverse particle sizes[47,48] it can be confirmed that the sample exhibits a slight hydrogen excess and hence it can be described as β-$NiOOH_{1+x}$ with x around 0.07. This is in agreement with the existence of a certain degree of solid solution formation for this phase that has been postulated to be close to 0.25 by different authors following the work of Barnard[48–50] but appeared to be slightly smaller than 0.1 from in situ neutron diffraction.[51]

DFT results and discussion of kinetics

Figure 4 illustrates calculated formation energies of T1 $Ni(OH)_2$, P3 NiOOH, and a variety of hydrogen configurations in TP2 $NiOOH_{1+x}$ (the formation energies are relative to T1 $Ni(OH)_2$ and the lowest energy P3 NiOOH ordering). A study of finite temperature phase stability in TP2 $NiOOH_{1+x}$ in principle requires a statistical mechanical approach to account for entropic contributions arising from the configurational disorder between hydrogen and vacancies[52,53] as well as the many tilt degrees of freedom of the primary H-O bonds.[54] Zero Kelvin formation energies, however, can already provide considerable insight about relative stability and solubility limits in the $Ni(OH)_2$-NiOOH system. Application of the common tangent construction to the formation energies shows that in thermodynamic equilibrium, hydrogen extraction from T1-$Ni(OH)_2$ will result in the formation of P3-NiOOH through a first-order phase transformation, as was predicted previously.[17] There are several energies plotted for P3-NiOOH, each corresponding to a different arrangement of primary H-O bonds in the prismatic edge sites of the intercalation layers.

The formation energies in Figure 4 clearly show that the experimentally observed TP2 form of NiOOH has a higher energy than P3 and is therefore metastable. The experimentally observed TP2 phase must therefore form as a result of kinetic factors that prevent the formation of the thermodynamically more favored P3 form of NiOOH. The lowest energy TP2 configuration at x = 0 may similarly be kinetically inaccessible because it involves a substantial

shearing of the layers: the alignment of "T1" layers in this configuration is approximately halfway between a T1 stacking and an O3 stacking. An analysis of phase stability between TP2 $NiOOH_{1+x}$ and T1 $Ni(OH)_2$, under the assumption that P3-NiOOH as well as the highly sheared TP2 configurations are kinetically suppressed, indicates that hydrogen removal from $Ni(OH)_2$ leads to the formation of TP2 with a hydrogen concentration in excess of that of NiOOH (i.e. $x > 0$). The corresponding common tangent construction is represented by the black line in Figure 4. TP2 $NiOOH_{1+x}$ is likely to exist as a solid solution below $x < 0.0833$. Although a full statistical mechanical treatment would be required to confirm this speculation, this is in full agreement with the results obtained from chemical analysis and from previous in situ neutron diffraction experiments.[51]

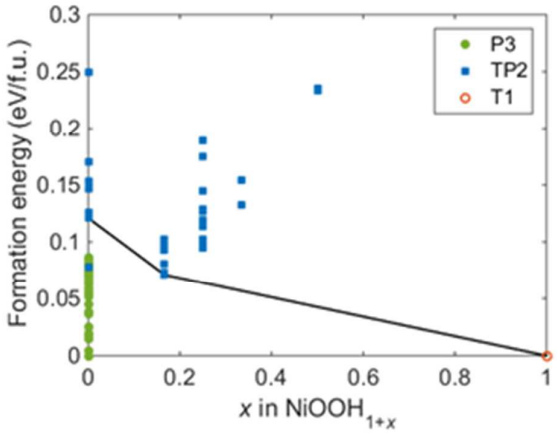

Figure 4. Formation energies of T1 (empty red circle), P3 (filled green circles) and TP2 (blue squares) structures at various hydrogen concentrations. The P3 phase is predicted to have the lowest energy at the NiOOH composition. Application of the common tangent construction within the assumption that formation of P3-NiOOH and highly sheared TP2-NiOOH upon hydrogen extraction from T1-$Ni(OH)_2$ is kinetically suppressed (solid line) shows that TP2 is hydrogen excess compared to NiOOH when in equilibrium with T1 $Ni(OH)_2$.

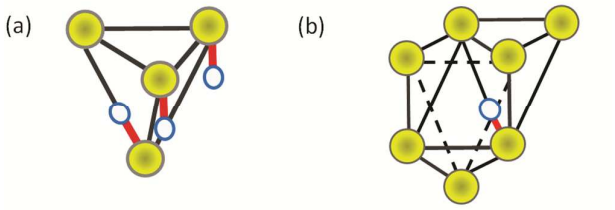

Figure 5: (a) Formation of hydrogen bond in a T environment as a result of hydrogen vacancies introduction, which according to DFT calculations allows tilting of primary H-O bonds. (b): Formation of hydrogen bond in a O environment as a result of the off-centering and hydrogen vacancies introduction, which according to DFT calculations allows tilting of primary H-O bonds (in red) resulting in the same structure as in a). White and yellow atoms represent H and O.

Hydrogen excess TP2 NiOOH is characterized by disorder in the tilt angles of the primary H-O bonds in the T-layers. If full occupation was considered, each hydrogen atom in the T layer, bound tightly to oxygen, would point towards the center of the tetrahedral site. If hydrogen vacancies are introduced in the T-layer, as is the case, symmetry is broken, and some oxygen ions will no longer have a primary bond with a hydrogen atom. These oxygen ions are then free to form secondary bonds with more distant hydrogen atoms, provided those more distant hydrogen atoms tilt from their ideal tetrahedral position, as illustrated in Figure 5 (a). The introduction of hydrogen vacancies in the ideal TP2 structure of $NiOOH_{1.5}$ can therefore lead to disorder in the orientation of the primary H-O bonds in the T-layers and to hydrogen bond formation, which would be consistent with FTIR results. If hydrogen atoms were to be placed in octahedral positions, hydrogen bond formation would only be possible if hydrogen atoms were off-centered and tilted from their ideal position.
Within this scenario, OP2 and TP2 polytypes would be equivalent (see figure 5b)). At the stoichiometric NiOOH composition in TP2, the lowest energy structure that is not highly sheared attains a high symmetry configuration whereby hydrogen atoms of the AA plane and of the BC plane bind to the same NiO_2 slab. In this structure, the H-O bonds of the T-layers now all direct themselves towards the centers of the tetrahedral sites.
The lowest energy structure obtained at $x = 0$ (shown in Figure 6) differs from those hypothesized previously[17,22,23] and involves a coupling between Jahn-Teller distortions and O-H bonds within the P3 host structure: the oxygen sites that are bonded to hydrogen participate in one short and two long Ni-O bonds, while the oxygen sites that are not bonded to hydrogen participate in three short Ni-O bonds. (See Supporting Information for structural details.) The stability of this ordering is consistent with valence bond sum considerations, as discussed previously in the case of $LiNiO_2$ and $NaNiO_2$.[55] We find that this structure is 161 meV/NiOOH more stable than the structure proposed by Tkalych et al.,[22] and 16 meV/NiOOH more stable than the charge-ordered structure proposed by Li et al.[23] (We constructed this charge-ordered structure using the occupation matrix control scheme described elsewhere.[55–57]) Although the lowest energy structure has a lower symmetry compared to the ideal P3 host, it does not have a doubled c-axis and possesses only one symmetrically unique H site.

NMR investigations

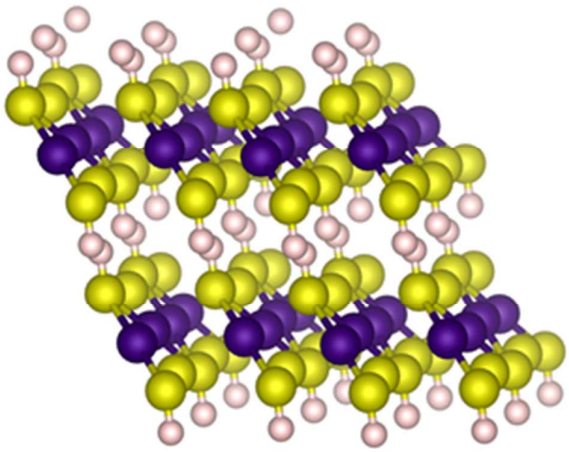

Figure 6. Distribution of hydrogen bonds and Jahn-Teller distortions within the P3 host for the lowest energy NiOOH structure. Pink, yellow and purple atoms represent H, O and Ni. . The orientation of the Jahn-Teller distortion at each site is indicated by bonds: long Ni-O bonds are shown while short Ni-O bonds are omitted. The dashed lines represent secondary O-H bonds.

The NMR spectra of β-NiOOD samples generally reveal the presence of more than one deuteron site. Four isotropic resonances are observed at 75, 5, -44, and -320 ppm in the ^{2}H MAS NMR spectrum of the sample prepared for the neutron diffraction experiments (Figure 7). The resonance at 5 ppm is assigned to mobile water (D_2O) molecules on the surface of the particles. The two strongest resonances at about 75 ppm and -44 ppm are present at a ratio of approximately 2:1 (75 : -44 ppm) on the basis of the deconvolution of the isotropic peaks and their spinning sidebands. The envelopes of the spinning sideband manifolds of these two resonances show a typical Pake-doublet, indicating that these two OD groups are rigidly bonded. A second sample of β-NiOOD had slightly different relative intensities for these peaks and hyperfine shift values, but again the approx. 75 ppm peak is more intense (see supplemental for its NMR spectrum, Figure S1b)). The peak at about -320 ppm is tentatively assigned to -OD groups in structural defects on the surfaces of the particles, due to its low concentration. The hyperfine shifts in paramagnetic materials depend strongly on the nature and number of nearby paramagnetic ions and also on the local coordination geometry. Assignments in this system are not trivial due to the effect that a small change in the Ni-OD bond angle will have on the shift of a Ni^{2+}/Ni^{3+} containing system and the effect of the Jahn-Teller distortion on the shift.[58] Deuterons in a stoichiometric crystalline sample of β-$Ni(OD)_2$, a material that adopts the brucite structure, resonate at -40 ppm (Figure S1 a)). Despite a resonance being observed at a similar shift in the spectrum of β-NiOOD, we do not believe this resonance arises from β-$Ni(OD)_2$ impurities in the β-NiOOD sample, because the average Ni oxidation state of this sample is very close to 3+. It is, however, tempting to assign the shift at -44 ppm to a T site resonance, (and thus the +75 ppm resonance

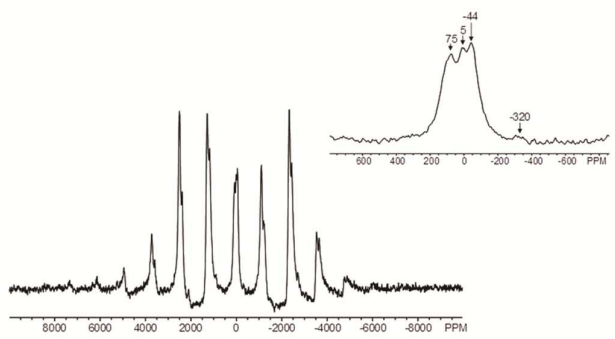

Figure 7: 2H MAS NMR spectrum of β-NiOOD. The isotropic resonances are labeled in the expansion of the spectrum shown in the inset; the remaining peaks are spinning sidebands.

to OD groups in the P layers). These assignments must remain tentative and therefore, the major conclusion that emerges from the NMR spectrum is that more than one structural deuteron site exists, which is not consistent with a simple P3 structural model (See SI for a discussion of aging and a more detailed discussion of NMR spectral assignments).

Rietveld refinement

Combined HRTEM and X-ray and neutron powder diffraction study of a β-NiOOH sample,[18] led to an average structure of the TP2 host type, resulting in a monoclinic C2/m unit cell, with irregular prismatic and tetrahedral hydrogen positions. In that study, stoichiometric β-NiOOH was considered, and tetrahedral hydrogen atoms were considered to be placed right above/below oxygen atoms of the BC interlayer and thus in a *4i* Wyckoff site, directing themselves towards the center of the tetrahedra.

In light of the analysis based on relative stabilities of structures and taking into account the plausible formation of hydrogen bonds, attempts were made to perform new refinements in order to more precisely refine hydrogen positions. Due to the incoherent neutron scattering length of hydrogen, the diffraction pattern of a deuterated sample was recorded. Refinement of this pattern led to an average crystal structure identical to the one obtained from the combined XRD/NPD refinement but some residual hydrogen was found to be left in the sample, causing difficulties in extracting additional information from a careful analysis of the hydrogen/deuterium positions. Thus, a new refinement was carried out with our pristine set of neutron data.

The scattering density (SD) Fourier difference maps calculated from the structural model proposed in our previous study[18] by suppressing hydrogen positions are depicted in Figure 8. Prismatic hydrogen atoms can be clearly identified on the (0 0 1) plane from the negative SD (Figure 8 (a)). These hydrogen atoms are approximately located on the edge of the prisms, coordinating to AA oxygen layers. These observations are in good agreement with DFT calculations, although in the maps an average position equidistant from the oxygen atoms above

Journal Name

ARTICLE

Atom	Wyckoff site	Occupancy	x/a	y/b	z/c	Biso (Å2)
Ni	4i	1	0.613(2)	1/2	0.2346(9)	3.1(3)
Oa	4i	1	0.958(2)	1/2	0.1304(8)	0.1(2)
Ob	4i	1	0.292(2)	1/2	0.370(1)	0.1(2)
HP	4i	0.5	0.492(6)	0	0.934(3)	0.1(2)
HT	8j	0.26	0.257(8)	0.14(1)	0.520(2)	0.1(2)

C2/m, a=4.881(2) Å b=2.908(3) Å c=9.254(4) Å β=88.59(4)°
Rp: 12.4, Rwp: 12.2, Rexp: 9.25, Chi2: 1.74
Table 1. Rietveld refined atomic parameters and unit cell of β-NiOOH.

and below is observed as a result of the different configurations available from off-centered sites. Figure 8 (b) shows the SD Fourier difference map (400) plane. Around z ≈ 0.5, a diffuse negative SD is also observed, that corresponds to hydrogen atoms between BC planes, confirming the existence of both types of hydrogen atoms. The fact that the scattering density is strongly diffuse could be indicative of a split position that is not exactly above/below oxygen atoms at y = 0. The tetrahedral hydrogen atoms are tilted pointing to oxygen atoms, as deduced based on DFT calculations for non-stoichiometric $NiOOH_{1+x}$.

Rietveld refinement was further carried out using NPD data by letting the position along the *b* axis of tetrahedral hydrogen atoms vary (fixed at y = 0 in the previous combined NPD/XRD refinement[13]). Hydrogen occupancies were constrained to the

Figure 8. Scattering density Fourier Difference maps calculated for (a) (001) plane and (b) planes perpendicular to a axis at x = 0.19, x = 0.25, x = 0.31. The negative SD (in cyan) corresponds to H atoms (see text).

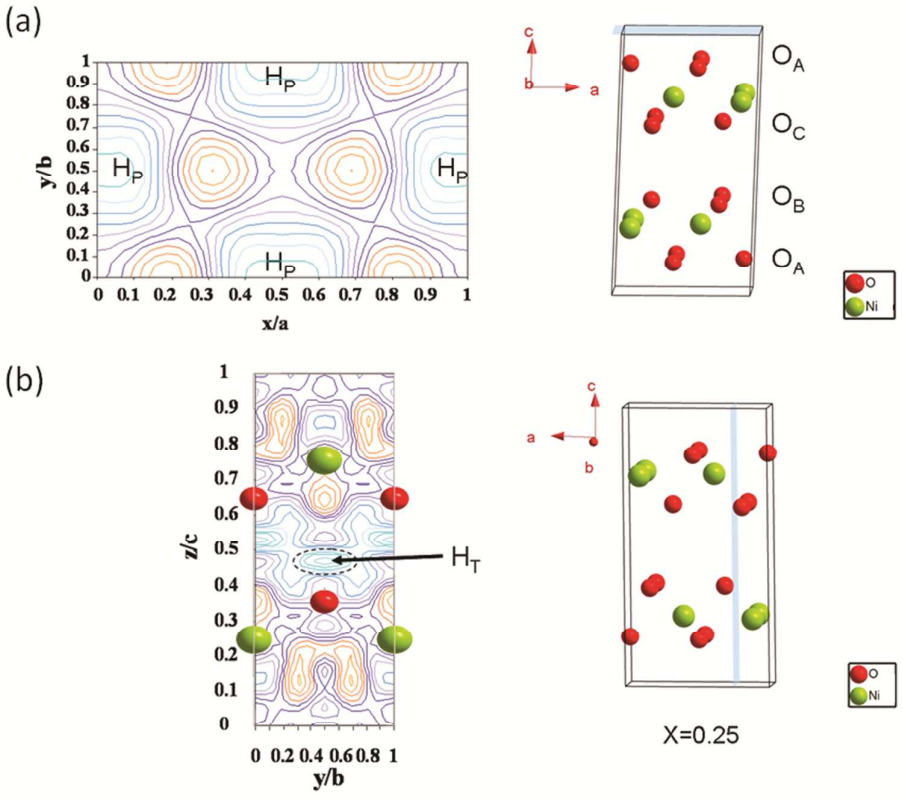

Journal Name

ARTICLE

Table 2. Selected atomic distances for β-NiOOH.

Atom 1	Atom 2	Count	Distance (Å)
Ni	Oa	2x	1.91(8)
	Oa	1x	1.92(1)
	Ob	1x	1.98(1)
	Ob	2x	2.12(1)
Ob	HT	2x	1.12(3)
	HT	2x	1.73 (3)
Oa	HP	1x	0.64(3)
	HP	1x	1.82 (3)
Ni	Ni	4x	2.84(1)
	Ni	2x	2.908(3)

value obtained from iodometric/complexometric titration. The refinement quickly converged to a split position for hydrogen atoms between BC planes (*8j* Wyckoff site with x = 0.257(8), y = 0.14(2), z = 0.520(2)) and prismatic hydrogen atoms slightly away from z = 0 (*4i* Wyckoff site with x = 0.492(6), y = 0 and z = -0.066(3)), and the final results are shown in table 1 and Figure 9. The represented unit cell corresponds to an average structure that results from the disorder in orientation of hydrogen bonds, with oxygen atoms bonding to a single hydrogen atom (either a primary or secondary hydrogen bond). Although there could be some mobility of tetrahedral hydrogen atoms along the *b* axis no evidence for significant mobility was found based on the NMR results. (Note that the timescale probed by the ^{2}H is on the order of 1-10 μs: slow motion must be occurring as the deuterons exchange with moisture in the air relatively rapidly on the timescale of hours to days (not quantified)). Hydrogen atoms in the BC interlayer form primary H-O bonds of 1.12 Å and secondary H-O bonds of 1.73 Å while prismatic hydrogen atoms would be bonding to oxygen atoms with a distance of 0.64 Å for primary bonds and 1.82 Å for secondary bonds. In both cases, H-O primary and secondary bonds are not expected to be exactly linear due to the strong distortions that the average structure exhibits. The H-O bond distances in prismatic hydrogen atoms are unlikely to be accurate (the primary H-O bond is too short), the error presumably arising because the electronic density is strongly diffuse, as observed in the Fourier difference map shown in Figure 8 a). A previous EXAFS study[59] concluded that the nickel-oxygen octahedra were distorted, with an average Ni-O distance of 1.92 Å distributed in four short distances (1.87 Å) and two long ones (2.03 Å). In our refined unit cell oxygen bond distances can also be separated into two groups leading to an average distance of 1.99 Å, and the Ni-O octahedra are less regular than previously reported (see table 2). The average

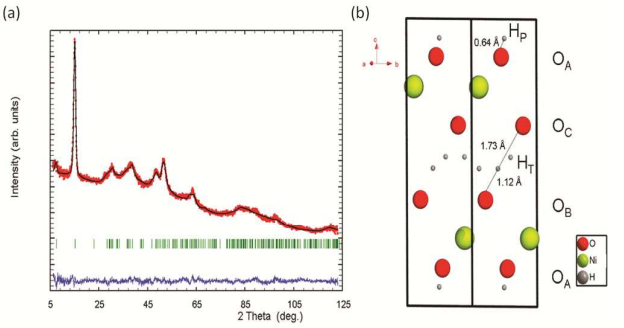

Figure 9. (a) Neutron powder diffraction patterns (small circles) showing the final Rietveld fit (solid line), with the difference pattern below. (b) Atomic representation of the Rietveld refined β-NiOOH unit cell.

Ni-Ni distance was found to be 2.86 Å, leading to four short distances of 2.84(1) Å and two long ones of 2.908(3) Å, in agreement with the EXAFS study that reported an average distance of 2.89 Å (4×2.82 Å and 2×3.03 Å).[59]

Kinetic origin of transformation to metastable TP2

We can understand the formation of TP2 NiOOH as opposed to the thermodynamically more favored P3 form upon hydrogen removal from $Ni(OH)_2$ by considering the physical mechanism with which the $Ni(OH)_2$ → NiOOH conversion occurs. Recent TEM images of nickel-hydroxide electrodes[18] have shown that the $Ni(OH)_2$ crystallites have nanometer dimensions. A schematic of a typical crystallite is illustrated in Figure 10(a), in which the NiO_2 slabs are discernible on the length scale of the crystallite. Both DFT formation energies and experimental voltage curve measurements, together with in situ neutron diffraction experiments,[51] indicate that the $Ni(OH)_2$ → NiOOH conversion occurs through a first-order phase transformation. This process is typically initiated by the nucleation of the new phase at the surface of the crystal lites, where the driving force for the transformation is the largest, followed by the inward migration of the interface separating the old phase from the growing phase. This is illustrated in Figure 10(b), where β-NiOOH forms at the surfaces of the crystallite upon hydrogen extraction, consuming the initial β-$Ni(OH)_2$ phase through the inward migration of an interface that separates β-NiOOH from β-$Ni(OH)_2$.

In large electrode crystallites, much of the kinetics of first-order phase transformations is dominated by long-range diffusion of the intercalating species (i.e. H or Li). However, in nanometer sized electrode crystallites, the interface plays a more significant role as its energetic contribution to the overall free energy of the particle relative to that of the bulk is

larger.[60] The interface can therefore be crucial in selecting out a particular kinetic pathway for the phase transformation. The transformation from T1 $Ni(OH)_2$ to either P3 or TP2 NiOOH requires a stacking sequence change, which should occur in a narrow region around the interface separating NiOOH from $Ni(OH)_2$ during the phase transformation. Transformation from T1 to P3 requires a shuffling of two out of every three NiO_2 slabs, while transformation from T1 to TP2 can occur through the shuffling of only every other NiO_2 slab (i.e. one out of every two). Interestingly, TP2 ABCA stacking sequences do locally exist in T1 as deformation stacking faults.[9,61] These misfit strains will be accommodated through elastic and possibly plastic deformations of the NiO_2 slabs in a region surrounding the interface. As less NiO_2 planes need to shuffle when transforming from T1 and TP2 compared to the T1 to P3 transformation, the interface separating T1 from TP2 should have a lower strain energy penalty than that between T1 and P3.

This difference in interface free energy is a possible origin of the formation of TP2 as opposed to the thermodynamically more stable P3 form of NiOOH. Although the free energy of the final state is lower when NiOOH adopts the P3 crystal structure, the smaller misfit strain between T1 $Ni(OH)_2$ and TP2 NiOOH are likely to lead to a more favorable free energy of two-phase coexistence in nano-crystallites during the transformation. The NMR results, which in the two samples we have investigated show two major resonances with intensities that are not 1:1, as would be expected for a TP2 model, suggest that on aging, some slow conversion of the TP2 phase to the P3 phase may occur, resulting in an increase in the ^2H resonance tentatively assigned to P3 deuterons. Although TP2 is metastable with respect to P3 and T1

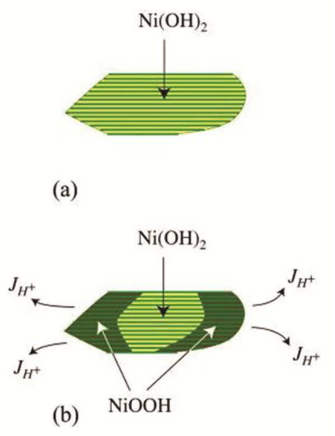

Figure 10: (a) Schematic illustration of a typical $Ni(OH)_2$ crystallite which has nanometer dimensions and clearly visible NiO_2 slabs (green lines) on the length scale of the particle dimensions. (b) Transformation of $Ni(OH)_2$ to NiOOH through a first order phase transformation upon hydrogen extraction occurs through the passage of an interface that migrates towards the interior of the crystallite converting $Ni(OH)_2$ to NiOOH (accompanied by hydrogen diffusion to the surface.

according to the convex hull shown in Figure 4, the calculations presented here do not allow us to definitively rule out the possibility that there exists some TP2 configuration that is low .enough in energy to be a thermodynamic ground state. Rigorously demonstrating that TP2 is metastable would require a thorough exploration not only of the degrees of freedom associated with vacancies and hydrogen bonds, but also the orientation of Jahn-Teller distortions and charge ordering of Ni ions. Systematically exploring all of these degrees of freedom computationally is possible[55] but beyond the scope of this work due to the large number of configurations.

Conclusions

In this paper we report a combined DFT, FTIR, NMR and NPD study in order to obtain further insight into the structure of β-NiOOH, which has been the topic of intense debate in the literature. Our work highlights the complementarity of the used techniques and demonstrates that disordered, nanometric materials can be fully characterized with an integrated approach.

β-NiOOH can be described as a TP2 oxygen host structure with excess hydrogen. The position of prismatic atoms has been unequivocally determined and found to be off-centered, as predicted by DFT. The location of tetrahedral hydrogen atoms is less straightforward due to the disorder in the tilt angles of hydrogen atoms. However, an average position on the edge of the tetrahedra was determined in which hydrogen atoms are tilted pointing to oxygen atoms forming quasi-linear hydrogen bonds. To our knowledge, this is the first layered material to exhibit TP2 type of oxygen packing. This form would have a kinetic origin and would be stabilised by the lower strain energy penalty existing in the T1-> TP2 transformation with respect to the T1-> P3 transformation. Interestingly, the confirmed shearing of the layers upon each oxidation/reduction reaction (proton deinsertion/insertion) does not prevent nickel batteries from having a long cycle life. This is expected to have relevant implications in the design intercalation compounds for alternative battery technologies (lithium, sodium, etc.) with mechanical stability towards structural changes and opens the door to the stabilization of other TP2 layered compounds. In turn, the full structural determination of β-NiOOH paves the way to rationalize its successful catalytic capability and the development of advanced electrocatalytic materials.

Conflicts of interest

There are no conflicts to declare.

Acknowledgements

The authors thank Dr. Juan-Rodríguez-Carvajal and Dr. Jesús Canales-Vázquez for fruitful discussions. MCC thanks the Departamento de Desarrollo Económico y Competitividad of

the Gobierno Vasco for financial Support and the Spanish Ministry for Economy, Industry and Competitiveness for grant ENE2016-81020-R. MRP acknowledges the Spanish Ministry for Economy, Industry and Competitiveness for the Severo Ochoa Programme for Centres of Excellence in R&D (SEV-2015-0496) and grant MAT2017-86616-R. CPG and JK thank the NSF for support via a collaborative research grant in chemistry, CHE0714183. MDR, AV and CPG were supported as part of the NorthEast Center for Chemical Energy Storage (NECCES), an Energy Frontier Research Center funded by the U.S. Department of Energy, Office of Science, Basic Energy Sciences under Award # DE- SC0012583. We acknowledge support from the Center for Scientific Computing from the CNSI, MRL: an NSF MRSEC (DMR-1121053), Hewlett-Packard, and the National Energy Research Scientific Computing Center (NERSC), supported by the Office of Science and U.S. Department of Energy, under Contract Number DE-AC02-05CH11231. We thank Drs. Y. Paik, F. Bardé, W. Bowden and F. Wang for providing the $Ni(OH)_2$ and one of the NiOOD samples and for running some of the NMR spectra.

Notes and references

1 163,170, 1901.
2 15,567, 1901.
3 157,290, 1901.
4 678,722, 1901.
5 P. Oliva, J. Leonardi, J. F. Laurent, C. Delmas, J. J. Braconnier, M. Figlarz, F. Fievet and A. de Guibert, *J. Power Sources*, 1982, **8**, 229–255.
6 S. U. Falk and A. J. Salkind, *Alkaline storage batteries*, Wiley, New York, 1969.
7 C. Greaves and M. A. Thomas, *Acta Crystallogr. B*, 1986, **42**, 51–55.
8 M. C. Bernard, R. Cortes, M. Keddam, H. Takenouti, P. Bernard and S. Senyarich, *J. Power Sources*, 1996, **63**, 247–254.
9 C. Delmas and C. Tessier, *J. Mater. Chem.*, 1997, **7**, 1439–1443.
10 C. Tessier, P. H. Haumesser, P. Bernard and C. Delmas, *J. Electrochem. Soc.*, 1999, **146**, 2059.
11 Z. S. Wronski, G. J. C. Carpenter and P. J. Kalal, in *Proc. 190th ECS Meeting*, San Antonio, 1996, pp. 96–14, 177.
12 M. Casas-Cabanas, J. Rodríguez-Carvajal, J. Canales-Vázquez and M. R. Palacín, *J. Mater. Chem.*, 2006, **16**, 2925–2939.
13 H. Bode, K. Dehmelt and J. Witte, *Zeitschrift Fur Anorg. Und Allg. Chemie*, 1969, **366**, 1–21.
14 O. Glemser and J. Einerhand, *Z. Anorg. Chem.*, 1950, **261**, 43–51.
15 H. Bartl, H. Bode, G. Sterr and J. Witte, *Electrochim. Acta*, 1971, **16**, 615–621.
16 S. Le Bihan, J. Guenot and M. Figlarz, *C. R. Acad. Sci. Ser. C*, 1970, **270**, 2131.
17 A. Van der Ven, D. Morgan, Y. S. Meng and G. Ceder, *J. Electrochem. Soc.*, 2006, **153**, A210–A215.
18 M. Casas-Cabanas, J. Canales-Vázquez, J. Rodríguez-Carvajal and M. R. Palacín, *J. Am. Chem. Soc.*, 2007, **129**, 5840–5842.
19 D. A. Corrigan and R. M. Bendert, *J. Electrochem. Soc.* , 1989, **136**, 723–728.
20 R. L. Doyle, I. J. Godwin, M. P. Brandon and M. E. G. Lyons, *Phys. Chem. Chem. Phys.*, 2013, **15**, 13737–13783.
21 O. Diaz-Morales, D. Ferrus-Suspedra and M. T. M. Koper, *Chem. Sci.*, 2016, **7**, 2639–2645.
22 A. J. Tkalych, K. Yu and E. A. Carter, *J. Phys. Chem. C*, 2015, **119**, 24315–24322.
23 Y. F. Li and A. Selloni, *J. Phys. Chem. Lett.*, 2014, **5**, 3981–3985.
24 V. Fidelsky, V. Butera, J. Zaffran and M. C. Toroker, *Theor. Chem. Acc.*, 2016, **135**, 162.
25 A. D. Doyle, M. Bajdich and A. Vojvodic, *Catal. Letters*, 2017, **147**, 1533–1539.
26 V. Fidelsky, D. Furman, Y. Khodorkovsky, Y. Elbaz, Y. Zeiri and M. Caspary Toroker, *MRS Commun.*, 2017, **7**, 206–213.
27 F. Bardé, M. R. Palacín, B. Beaudoin and J. M. Tarascon, *Chem. Mater.*, 2005, **17**, 470–476.
28 J. Rodríguez-Carvajal, *Phys. B Condens. Matter*, 1993, **192**, 55–69.
29 P. Thompson, D. E. Cox and J. B. Hastings, *J. Appl. Crystallogr.*, 1987, **20**, 79–83.
30 G. Kresse and J. Hafner, *Phys. Rev. B*, 1993, **47**, 558–561.
31 G. Kresse and J. Hafner, *Phys. Rev. B*, 1994, **49**, 14251–14269.
32 G. Kresse and J. Furthmüller, *Comput. Mater. Sci.*, 1996, **6**, 15–50.
33 G. Kresse and J. Furthmüller, *Phys. Rev. B*, 1996, **54**, 11169–11186.
34 J. Klimeš, D. R. Bowler and A. Michaelides, *Phys. Rev. B*, 2011, **83**, 195131.
35 M. Dion, H. Rydberg, E. Schröder, D. C. Langreth and B. I. Lundqvist, *Phys. Rev. Lett.*, 2004, **92**, 246401.
36 J. Klimeš, D. R. Bowler and A. Michaelides, *J. Phys. Condens. Matter*, 2010, **22**, 022201.
37 S. Dudarev, G. Botton, S. Savrasov, C. Humphreys and A. Sutton, *Phys. Rev. B*, 1998, **57**, 1505–1509.
38 F. Zhou, M. Cococcioni, C. Marianetti, D. Morgan and G. Ceder, *Phys. Rev. B*, 2004, **70**, 235121.
39 P. E. Blöchl, *Phys. Rev. B*, 1994, **50**, 17953.
40 P. Blöchl, O. Jepsen and O. Andersen, *Phys. Rev. B*, 1994, **49**, 16223–16233.
41 *CASM, v0.2.0, 2016. Available from https// github.com/prisms-center/CASMcode*, DOI:10.5281/zenodo.60142.
42 J. C. Thomas and A. Van Der Ven, *Phys. Rev. B*, 2013, **88**, 214111.
43 B. Puchala and A. Van Der Ven, *Phys. Rev. B*, 2013, **88**, 094108.
44 A. Van der Ven, J. C. Thomas, Q. Xu and J. Bhattacharya, *Math. Comput. Simul.*, 2010, **80**, 1393–1410.
45 R. Mechanism and E. Properties, *J. Electrochem. Soc.*, 1997, **144**, 4226–4236.
46 F. P. Kober, *J. Electrochem. Soc.*, 1967, **114**, 215.

47 M. R. Palacín, D. Larcher, A. Audemer, N. Sac-Épée, G. G. Amatucci and J. -M. Tarascon, *J. Electrochem. Soc.* , , DOI:10.1149/1.1838171.

48 R. Barnard, C. F. Randell and F. L. Tye, *J. Appl. Electrochem.*, 1980, **10**, 109–125.

49 K. Süvegh, T. S. Horanyi and A. Vértes, *Electrochim. Acta*, 1988, **33**, 1061–1066.

50 C. Léger, C. Tessier, M. Ménétrier, C. Denage and C. Delmas, *J. Electrochem. Soc.*, 1999, **146**, 924–932.

51 F. Bardé, M. R. Palacin, Y. Chabre, O. Isnard and J. M. Tarascon, *Chem. Mater.*, 2004, **16**, 3936–3948.

52 Q. Xu and A. Van Der Ven, *Phys. Rev. B*, 2007, **76**, 064207.

53 A. Van der Ven, J. C. Thomas, Q. Xu, B. Swoboda and D. Morgan, *Phys. Rev. B*, 2008, **78**, 104306.

54 T. Mueller and G. Ceder, *Phys. Rev. B - Condens. Matter Mater. Phys.*, , DOI:10.1103/PhysRevB.74.134104.

55 M. D. Radin and A. Van der Ven, *Chem. Mater.*

56 B. Dorado, B. Amadon, M. Freyss and M. Bertolus, *Phys. Rev. B*, 2009, **79**, 235125.

57 J. P. Allen and G. W. Watson, *Phys. Chem. Chem. Phys.*, 2014, **16**, 21016–21031.

58 D. Carlier, M. Ménétrier, C. P. Grey, C. Delmas and G. Ceder, *Phys. Rev. B*, 2003, **67**, 174103.

59 A. Demourgues, L. Gautier, A. V. Chadwick and C. Delmas, *Nucl. Instruments Methods Phys. Res. Sect. B*, 1997, **133**, 39–44.

60 M. Wagemaker, F. M. Mulder and A. Van Der Ven, *Adv. Mater.*, 2009, **21**, 2703–2709.

61 M. T. Sebastian and P. Krishna, *Random, non-random, and periodic faulting in crystals*, Gordon and Breach Science Publishers, Yverdon, Switzerland; Langhorne, Penn., 1994.

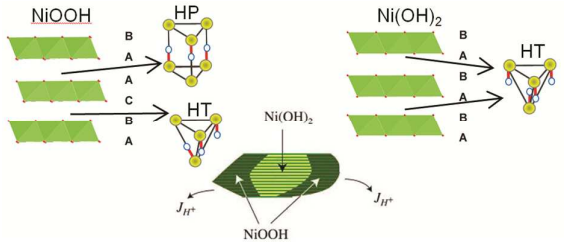

β-NiOOH crystallizes in a TP2 structure where both T and P hydrogen atoms form primary and secondary H-bonds with oxygen.